Corrosion Science xxx (2016) xxx–xxx

Contents lists available at ScienceDirect

Corrosion Science

journal homepage: www.elsevier.com/locate/corsci

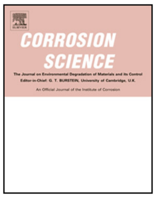

Oxidation of a Fe–18Cr–8Ni austenitic stainless steel at 850 °C in O_2: Microstructure evolution during breakaway oxidation

Audrey Col, Valérie Parry, Céline Pascal*

Univ. Grenoble Alpes, CNRS, SIMaP, F-38000 Grenoble, France

ARTICLE INFO

Article history:
Received 7 July 2016
Received in revised form 8 October 2016
Accepted 16 October 2016
Available online xxx

Keywords:
A. Stainless steel
B. Raman spectroscopy
B. SEM
B. TEM
C. Internal oxidation
C. High temperature corrosion

ABSTRACT

Oxidation tests of AISI 304L in breakaway conditions (850 °C in O_2) were performed up to 312 h. The evolution of the oxidation affected zone microstructure was investigated using a combination of composional/elemental (TEM, Raman spectroscopy) and structural (EBSD) mapping techniques as well as thermodynamic calculations. The formation of a dense and continuous Cr_2O_3 healing layer at the border of the internal oxidation zone happens along the grain boundaries and is linked to their more efficient Cr supply. The propagation of the oxidation front is related to a local conversion of Cr_2O_3 in less protective $FeCr_2O_4$.

1. Introduction

Austenitic stainless steels, such as AISI 304L, are protected from rapid oxidation by the selective consumption of chromium which leads to the formation of a protective chromia scale, Cr_2O_3, characterised by a slow growth rate. Numerous investigations related to chromia forming alloys report the formation of a two-layer oxide scale composed of a dense and adherent inner sub-layer of Cr_2O_3 and an outer sub-layer of spinel type oxide $MnCr_2O_4$ [1–4]. Chromia is a barrier against further oxidation owing to its very low diffusion coefficients for oxygen and metals, and then offer a high oxidation resistance [5].

The formation of protective Cr-rich oxide scale, Cr_2O_3, depends on the chromium concentration at the alloy/oxide interface and also on the chromium diffusion coefficient in the metallic substrate from the core towards the interface. Analytical solutions of the Wagner's equations have been used to model the Cr depletion profiles [6,7]. According to Evans et al. experiments [8], about 16 wt.% in Cr is required at the alloy/scale interface to form a healing layer in the temperature range from 750 to 900 °C for a Fe–20Cr–25Ni steel. However, the steel grain size [2,9–14], the silicon content in the alloy [12,15–17] and the surrounding atmosphere [18] influence the Cr critical value for a given temperature. Decreasing the alloy grain size allows a quicker formation of a continuous chromia layer due to a faster effective diffusion of Cr in the alloy and to a smaller lateral growth distance required to form a continuous layer. Presence of silicon in the nominal composition of the steel induces the formation of silica at the alloy/oxide interface that acts as an additional diffusion barrier. In water vapour [19–22] or carbon dioxide [23,24] containing atmospheres, the growth rate of chromia scale is increased causing a greater depletion of Cr in the subsurface zone. In both cases, the subsequent loss of chromium tends to convert the protective Cr-rich oxide, initially formed, into a poorly protective Fe-rich fast growing oxide [25,26]. Moreover, part of Cr can be either trapped in $M_{23}C_6$ or M_7C_3 carbides in carburizing atmospheres [27,28], or lost through Cr_2O_3 volatilization in gaseous $CrO_2(OH)_2(g)$ in water vapour containing atmospheres [29,30].

According to Huntz et al. [3], for austenitic stainless steels, 18 wt.% of Cr is not sufficient to sustain the formation of chromia when temperature (or time) increases because lattice diffusion coefficients in face-centered cubic crystal structure (fcc-austenite) are smaller than the one in body-centered cubic crystal structure of ferritic stainless steel (bcc-ferrite). At high temperature (>850 °C) in high oxygen partial pressure (O_2 or air), even if a thin chromia scale forms in the early stage of oxidation, the chromium concentration and diffusivity cannot feed the further growth of Cr_2O_3. Then, the nodular growth of iron oxides (spinel-like phase and hematite) takes place which induces a sudden increase of the oxidation rate. The phenomenon is usually called "breakaway oxidation".

---

* Corresponding author.
E-mail address: Celine.Pascal@simap.grenoble-inp.fr (C. Pascal).

http://dx.doi.org/10.1016/j.corsci.2016.10.029

Please cite this article in press as: A. Col, et al., Oxidation of a Fe–18Cr–8Ni austenitic stainless steel at 850 °C in O_2: Microstructure evolution during breakaway oxidation, *Corros. Sci.* (2016), http://dx.doi.org/10.1016/j.corsci.2016.10.029

In various experimental conditions, breakaway oxidation of austenitic stainless steels gives rise to the inward growth of a complex oxide composed of a (Ni,Fe)-rich phase and of a spinel type oxides: in carburizing atmospheres [23,24,26,27,31], in water vapour containing atmospheres [25,30,32–37] and in air at higher temperature [4]. In all cases, depletion of chromium in the subsurface alloy zone is the key factor leading to breakaway oxidation. Depending on the experimental conditions, Ni-rich phase trapped in $FeCr_2O_4$ spinel oxide may be metallic or oxidised: $(Ni,Fe,Cr)_3O_4$ spinel oxide [25,26,36], $FeNi_3$ [31], Ni–Fe solid solution [4,23,33,35,37–39]. Some authors also report formation of a Cr-rich oxide layer at the interface with the substrate which can be Cr_2O_3 [23,30,40] or $FeCr_2O_4$ [35,37].

The objective of this work is to study the evolution of the AISI 304L microstructure after breakaway oxidation in oxygen at 850 °C, to characterise the observed microconstituents and to describe the breakaway process in such experimental conditions. In particular, Raman spectral mapping allows to evidence an alteration of the composition from Cr_2O_3 to $FeCr_2O_4$ linked to a loss of protectiveness of the Cr-rich oxide scale formed at the interface with the substrate.

2. Material and methods

The commercial 1 mm-thick foil of AISI 304L (EN 1.4307) used in this work was supplied by Goodfellow. The chemical composition obtained by fluorescence spectroscopy analysis and optical emission spectrometry equipped with a gas analyser is reported in Table 1.

Specimens were cut to $10 \times 20 \times 1\ mm^3$ dimensions, then ground up to 1200 grit with SiC abrasive papers. After measurement of dimensions, the coupons were cleaned in acetone and ethanol.

Oxidation experiments were performed in a tubular furnace at 850 °C (heating rate 13 °C/min) at atmospheric pressure in O_2 gas flow (flow speed of 21 cm/min at room temperature) for 48–312 h. The samples were placed in several ceramic boats to take them out after a given time. Short-time oxidized samples (48 h, 72 h and 96 h) were quenched under a continuous flow of O_2 in the cold extremity of the furnace. Long-time oxidized samples (110 h, 120 h, 148 h and 312 h) were naturally cooled down in the furnace under O_2 flow in order to limit the spallation of their thicker oxide scales due to the mismatch of thermal expansion coefficients between the oxide scale and the metallic substrate.

After oxidation, sample cross-sections were prepared for microstructural investigations. Samples were coated using epoxy resin to prevent oxide scale damages during metallographic preparation (cutting, grinding and polishing). The sample cross-sections were ground up to 1200 grit SiC paper and polished up to 1 μm diamond paste.

A first set of two techniques was used to characterize of the oxide phases that are present on the outer surface of the oxide scale. Raman spectroscopy was performed on the oxidized sample surface in order to determine the chemical composition of the oxide phase (spatial resolution ~1 μm^2 with depth resolution ~1 μm). For each sample, ten Raman spectra were randomly acquired with a Renishaw RM1000 spectrometer using a 514.532 nm Ar-laser. The morphology of the outer oxide scale was investigated using scanning electron microscopy (SEM, LEO S440).

A second set of techniques was carried out to study the complex chemistry and morphology of the oxidation affected zone on cross-sections. Observations were performed using a Field Emission Gun (FEG) SEM Zeiss Ultra 55 equipped with a X-Ray (SSD Bruker) detector and an Electron Back Scattered Diffraction (EBSD, TSL-EDAX) detector. Identification of oxide composition was carried out using Raman spectral mapping. Due to the spatial resolution limits of the SEM and Raman spectroscopy techniques, elemental chemical analysis of the finest microconstituents was performed with transmission electron microscopy (TEM). The TEM thin lamella was prepared using focused ion beam thinning (SEM-FIB Zeiss Nvision 40) and observed using a TEM-FEG Jeol 2100F equipped with EDS analysis. The chemical composition in the underlying substrate was analysed using electron probe microanalysis (EPMA, Cameca SX50).

3. Results

3.1. Evolution of microstructure and composition of the outer oxides scale

SEM surface views in SE mode of the AISI 304L specimens oxidized at 850 °C in O_2 for 48–312 h are displayed in Fig. 1. For the shorter oxidation times (48 h, 72 h and 96 h), the oxide surface is smooth with submicronic polygonal grains. Local thickenings occur after 96 h of oxidation. For oxidation time longer than 110 h, oxide morphology is strongly modified with the appearance of coarse angular crystals. Formation of necks between grains happens leading to a porous sintered-like microstructure of the base oxide. After 312 h at 850 °C, the oxide scale is rough with formation of nodules and vertical growth of oxide grains.

For oxidation time longer than 110 h, the oxide scale is thick and porous, sign of a rapid oxide growth. The thermal stresses, originated from the mismatch of the thermal expansion coefficients between the oxide and the alloy, associated with a low cohesive energy of the porous oxide result in oxide spallation during cooling.

Surface Raman spectra of the samples oxidized for 72 h and 312 h at 850 °C in O_2 are displayed in Fig. 2. For each samples, ten spectra were randomly acquired. Raman peaks were identified using McCarthy and Boehme [41] and Hosterman spectra as references [42].

According to Fig. 2a, for 90% of spectra, the outer oxide scale after 72 h at 850 °C is composed of corundum-structure solid solution $Fe_{2-x}Cr_xO_3$ with varying composition up to Fe-rich one. Small amounts of chromia Cr_2O_3 and manganese chromite $MnCr_2O_4$ are also detected (10% of spectra in Fig. 2b).

Since a partial spallation of the oxide scale occurs for the longest oxidation time, two types of spectra were recorded for the sample oxidized for 312 h. The outer oxide scale, related to an unspalled area in Fig. 2c, is mainly composed of hematite Fe_2O_3 with a small amount of Fe-rich corundum-type solid solution $Fe_{2-x}Cr_xO_3$. According to Fig. 2d, spalled areas contain Fe–Cr spinel-type oxide which indicates that spallation happens within the oxide scale rather than at the alloy/oxide interface. These results show that the oxide scale is duplex with formation of hematite on the top surface and of Fe–Cr spinel-type oxide as inner scale, as typically reported in literature [1,3,4,43,44].

SEM outer surface study associated to Raman spectroscopy results allow to describe the chemical and morphological evolution of the outer surface of the oxide scale during oxidation of AISI 304L at 850 °C in O_2.

Up to 96 h, the oxide scale is made of regular platlet grains of corundum-structure solid solution $Fe_{2-x}Cr_xO_3$. The iron content

Table 1
Chemical composition of austenitic stainless steel AISI 304L (in wt.%).

wt.%	Fe	Ni	Cr	Mn	Si	Co	Cu	Mo	C	S
AISI 304L	Bal.	8.143	17.462	1.724	0.319	0.203	0.355	0.262	0.021	0.002

Please cite this article in press as: A. Col, et al., Oxidation of a Fe–18Cr–8Ni austenitic stainless steel at 850 °C in O_2: Microstructure evolution during breakaway oxidation, *Corros. Sci.* (2016), http://dx.doi.org/10.1016/j.corsci.2016.10.029